RUSSIAN JOURNAL OF EARTH SCIENCES
vol. 19, 3, 2019, doi: 10.2205/2019ES000661

Infrasound induced plasma perturbations associated with geomagnetic pulsations

Justin Mabie[1,2]

[1]Cooperative Institute for Research in Environmental Sciences, University of Colorado Boulder, Boulder, Colorado, USA

[2]National Centers for Environmental Information, National Oceanic and Atmospheric Administration, Boulder, Colorado, USA

Abstract. Experiments were conducted to observe infrasound induced plasma displacements and variations in HF radio propagation and absorption in the ionosphere after rocket launches. Variations in HF echo arrival angle and received power are observed and are consistent with the periods of PC1 pulsations. Plasma displacements consistent with the periods of PC3 pulsations were observed and associated with rocket induced infrasonic waves. These observations help develop our understanding of how infrasonic waves that originate near the ground, exchange energy with the geomagnetic field at high altitudes and how the geomagnetic field responds to them.

This is the e-book version of the article, published in Russian Journal of Earth Sciences (doi:10.2205/2019ES000661). It is generated from the original source file using LaTeX's **ebook.cls** class.

Key Points

1. Infrasonic wave induced plasma displacements with periods consistent with PC3 oscillations are observed.
2. Phase coherent changes in HF radio propagation path and absorption consistent with PC1 oscillations are observed.
3. Possible causes of infrasound induced PC5 pulsations are discussed.

Introduction

This paper aims to identify plasma signatures that may be related to geomagnetic pulsations caused by infrasonic waves that propagate from near the ground into the thermosphere. These High Altitude Acoustic Waves (HAAW) are infrasonic waves known to cause ionospheric disturbances that can be observed with ionosondes [*Mabie et al.*, 2016; *Maruyama et al.*, 2012] and cause geomagnetic pulsations that have been observed with magnetometers [*Toshihiko et al.*, 2005]. Geomagnetic pulsations can also be detected by ionospheric sounders [*Sutcliffe and Jarvis*, 1996] and space-

based instruments [*Yagova et al.*, 2015]. Geomagnetic pulsations are classified by their period and properties as defined by the International Association of Geomagnetism and Aeronomy (IAGA) [*Saito*, 1978] and their energy can be distributed by the Ionospheric Alfvén Resonator (IAR) [*Nosé et al.*, 2017]. The classes and respective periods of Pulsations Continuous (PC) of interest are PC1 (0.2 s–5 s), PC3 (10 s–45 s) and PC5 (150 s–600 s). Identification of the class and proposed cause of possible geomagnetic pulsations after rocket launches is presented.

Experiments were conducted to measure Line Of Sight (LOS) plasma displacements and variations in High Frequency (HF) radio wave propagation and absorption caused by rocket induced HAAW. Observations were made with the NASA Wallops Flight Facility (WFF) Vertically Incident Pulsed Ionospheric Radar (VIPIR). The results are from three experiments conducted during the flights of the Orbital Corporation Antares missions OA-8, ORB-1 and ORB-3. These HAAW are generated when the rocket clears the launch pad and the rocket exhaust reverberates off of the ground. These rocket induced HAAW propagate in the vertical direction and cause the observed LOS plasma displacements in the ionosphere. They are classified as infrasonic

waves based on their propagation speed and period [*Wickersham,* 1966]

The connection between VIPIR ionosonde observations and geomagnetic pulsations is inferred. Geomagnetic pulsations are not themselves detected, but the presented observations are considered evidence of their presence.

The WFF VIPIR Ionosonde

The WFF VIPIR usually functions as an advanced ionosonde which takes advantage of an optimized field site [*Pitteway and Wright,* 1992] and Dynasonde analysis software [*Zabotin et al.,* 2006]. The VIPIR is unique in its ability to operate in different user defined modes. For the presented observations the VIPIR is programmed into a mode where fixed frequency pulses are interleaved with a modified Dynasonde mode sweep frequency pulse set [*Mabie et al.,* 2016]. This mode allows for determination of an extensive suite of ionospheric properties including the Electron Density Profile (EDP) while also making high temporal resolution observations of individual plasma layers.

LOS plasma displacements are Doppler velocity mea-

surements of electron motion, computed using the phase progression of the fixed frequency observations. To first order these values represent actual plasma displacements, but error can be introduced by phase changes that are not caused by plasma motion [*Bianchi and Altadill,* 2005].

Variations in received power are taken to be caused by modulations of radio wave absorption that occurs near the radio wave reflection point (deviative absorption) and away from the reflection point. In this study, observed oscillations in received power that are of interest are taken to be caused by plasma induced oscillations near the reflection point. These can be caused by local changes in the EDP or in the radio wave propagation path. Variations in absorption occur under normal atmospheric conditions and are predicted by the Appleton-Hartree equation [*Pederick and Cervera,* 2014; *Scotto and Settimi,* 2014].

Arrival angles of VIPIR echoes are computed through interferometry across the VIPIR receive array. The arrival angle is the result of the cumulative propagation path of the radio wave through the atmosphere. Individual phase values used to compute arrival angle are subject to errors caused by limitations of the radar electronics and environmental radio noise but are mini-

mized by the high Signal to Noise Ratio (SNR) of VIPIR echoes. Variations in arrival angle are assumed to be caused by plasma structure in the ionosphere which changes the index of refraction and the resulting radio wave propagation path. This is a cumulative effect subject to irregularities at all ionospheric altitudes below the radio wave reflection point and can be highly variable even during relatively calm environmental conditions. The small oscillations consistent with PC1 pulsations shown in Figure 1 and Figure 2 are relatively small compared to typical variations in arrival angle and their detection can be easily obscured by normal ionospheric variability.

The VIPIR receive array is oriented in the geographic East–West $\hat{x}$ and North–South $\hat{y}$ directions. The geomagnetic field at the nominal observation altitude of 150 km above WFF has a declination of -11.1° and an inclination of 64.4°. Observations made in the $\hat{x}$ direction are nearly perpendicular to and observations made in the $\hat{y}$ direction are nearly parallel to the geomagnetic field.

The observed HAAW induced variations in arrival angle are within a few degrees off of zenith. Because of this, the radio wave propagation path can be assumed to be in the vertical direction $\hat{z}$. In contrast, even small

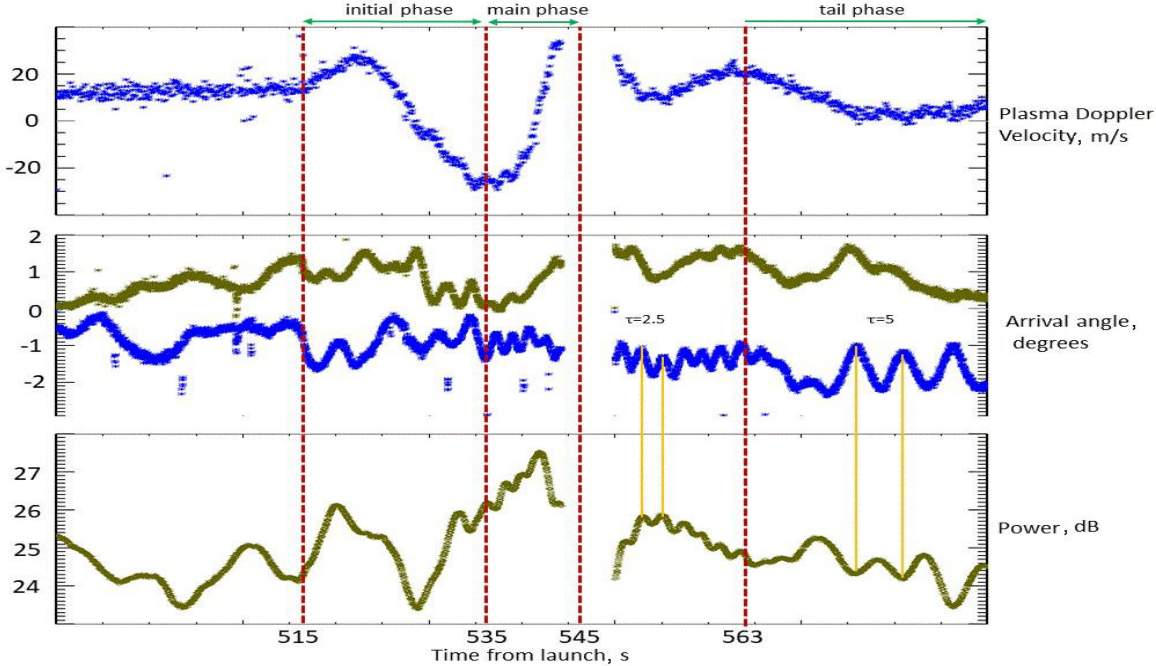

Figure 1. OA8 observations of A) LOS plasma Doppler velocity B) arrival angle in the East–West direction (blue) and the North–South direction (green) and C) received power during passage of the HAAW generated by the OA8 rocket engines. A 2.5 s phase coherent oscillation is present in the East–West component of arrival angle and received power as the HAAW passes. During the tail period a 5 s phase coherent oscillation is seen in both arrival angle and received power. Initial, main and tail phases of HAAW passage are identified.

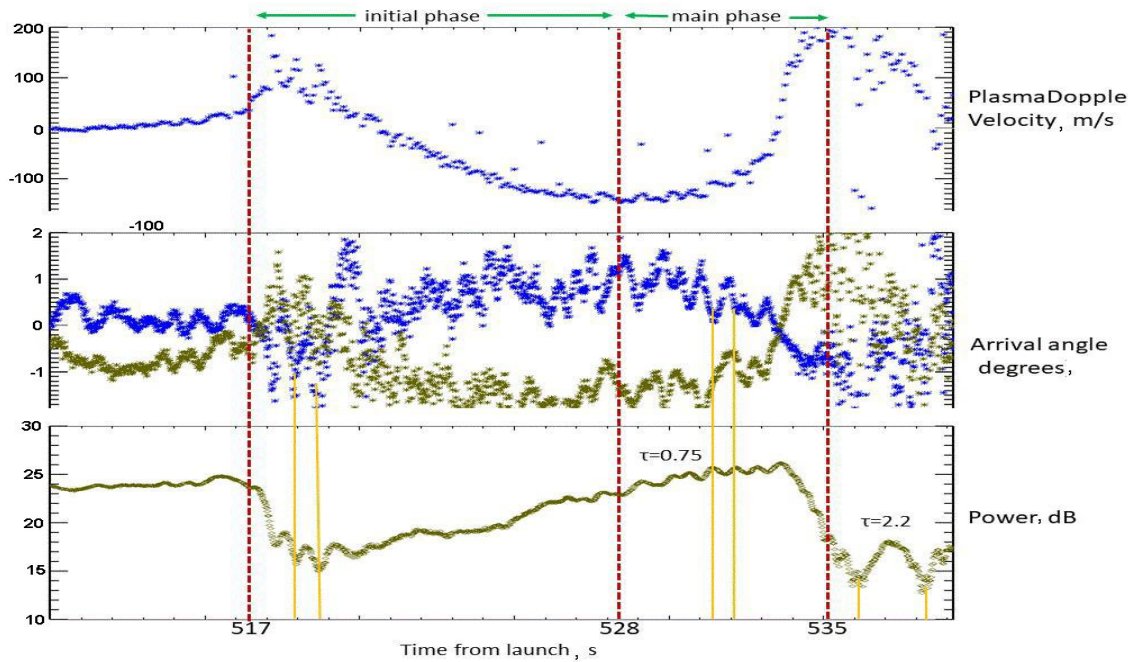

Figure 2. ORB1 observations of A) LOS plasma Doppler velocity B) arrival angle in the East–West direction (blue) and the North–South direction (green) and C) received power during passage of the HAAW generated by the ORB1 rocket engines. A 0.75 s phase coherent oscillation can be seen in the East–West component of arrival angle and received power as the HAAW passes. A 2.2 s oscillation can be seen in received power just after the main phase. Initial and main phases of HAAW passage are identified.

changes in arrival angle represent variations that occur in the horizontal directions. Variations in radio wave propagation can occur near the radio wave reflection point (deviative) or away from the radio wave reflection point. Arrival angle oscillations of one or two degrees must be interpreted carefully because variations are expected to be present in VIPIR data during most ionospheric conditions [*Negrea et al.*, 2016].

The presented VIPIR observations have a pulse repetition of 10 ms and a 10 μs range gate sampling interval. There is a fixed frequency pulse and resulting value of received power and arrival angle every 20 ms and a LOS plasma Doppler velocity value every 80 ms. Each minute the VIPIR transmits for 50 s followed by a ten second period when no observations are made.

Observations

The observed HAAW induced LOS plasma displacements are characterized by an initial upward plasma displacement, followed by relatively large amplitude downward and upward plasma displacements, followed by a relaxation period where the plasma is restored to predisturbance conditions. The passage of a rocket induced HAAW through a plasma layer is identified in

terms of three phases defined by the plasma displacements. An example of the plasma displacements and phases of HAAW passage are illustrated in Figure 1. The initial phase begins with the initial upward plasma displacement and ends with the large amplitude downward plasma displacement peak. The main phase begins with the large amplitude downward plasma displacement peak and ends with the large amplitude upward plasma displacement peak. The tail phase begins with the final HAAW induced plasma displacement peak which is either the large amplitude upward plasma displacement peak, or when additional oscillations are present it is the last HAAW induced plasma displacement peak. The end of the tail phase is defined as when the plasma is no longer disturbed by the HAAW, but can be difficult to positively identify because of the presence of other disturbances, especially gravity waves which are almost always present [*Negrea and Zabotin,* 2016].

The presented ionosonde observations include plasma displacements that may induce geomagnetic pulsations. They also include changes in the arrival angle and received power of HF echoes that may be caused by those geomagnetic pulsations.

The observations shown in all figures are presented

in seconds from launch time. LOS plasma Doppler velocity is in the vertical ($\hat{z}$) direction. Arrival angle is in the horizontal directions where the blue trace is in the East–West ($\hat{x}$) direction and the green trace is in the North–South ($\hat{y}$) direction.

OA-8 Observations

The Orbital corporation Cygnus CRS OA-8E Space Station Cargo Resupply Antares rocket (OA-8) was launched 12 November 2017 at 12:19:51 UTC (07:19 AM local time). Observations made during the OA-8 flight are a good example of the experimental results. At the time of the launch ionospheric soundings show a weak E layer and a typical undisturbed $F1$ layer. The $F2$ layer had a highly structured lower boundary but was otherwise unstructured. A single fixed frequency of 3274 kHz was used to observe the plasma layer at 190 km altitude.

In Figure 1, the main phase of HAAW passage is identified by the large-amplitude downward and upward plasma displacement peaks that occur at $T+535$ s and $T+545$ s respectively. This corresponds to a wave period of 20 s consistent with the period of a PC3 pulsation. The large-amplitude upward plasma displace-

ment peak arrival time is interpolated because it occurred during a ten second period when the VIPIR is not transmitting.

Phase coherent oscillations are identified in both received power and the $\hat{x}$ component of arrival angle with a period of 2.5 s during and shortly after the main phase of the HAAW passage. During the tail phase, there is an observed phase coherent oscillation having an initial period of 5 s which increase to almost 7 s as the HAAW moves away from the observation altitude. These periods are consistent with the periods of PC1 pulsations.

ORB-1 Observations

The Orbital Corporation Cygnus CRS ORB-1 cargo resupply Antares rocket (ORB-1) was launched 9 January 2014 at 18:07:05 UTC (13:07 local time). The conditions were typical of a January mid-day ionosphere with $E1$, $F1$ and $F2$ layers present with an additional cusp below $F1$. Some E layer spread is present within a relatively undisturbed ionosphere. A single fixed frequency of 4165 kHz was used to observe the plasma layer at 156 km altitude.

In Figure 2, the main phase of the ORB-1 HAAW passage is identified by the downward and upward plasma

displacement peaks that occur at $T + 528$ s and $T + 535$ s respectively. The main phase covers half the 14 s wave period which is consistent with the period of a PC3 pulsation.

During the main phase of HAAW passage, phase coherent oscillations are observed in both received power and the $\hat{x}$ component of arrival angle having a period of 0.75 s. After passage of the main phase, a 2.2 s oscillation is observed. Within the margin of error, this is an integer multiple of three from the 0.75 s phase coherent oscillation. These periods are consistent with the periods of PC1 pulsations.

ORB-3 Observations

The Orbital Corporation Cygnus CRS Flight 3 (ORB-3) resupply Antares rocket was launched 28 October 2014 at 22:22:38 UTC (18:22 local time). This was early evening, after sunset with an E layer and some sporadic-E still present. A single F layer was present with the peak plasma frequency (f_oF2) near 10 MHz. A radar clock error was discovered after the ORB-3 observations and launch time is adjusted by assuming the HAAW propagates at the adiabatic speed of sound until it is identified at 201 km altitude. Three fixed frequen-

cies were used at 3290 kHz, 5230 kHz and 6810 kHz to observe the plasma layers at 201 km, 217 km and 233 km respectively.

Figure 3, Figure 4 and Figure 5 show variations in echo arrival angle and the plasma displacements at each frequency. Echo power is not displayed because ORB-3 was a night time launch where there is no discernible *D*-region absorption because of the lack of plasma in the ionospheric *D*-region. The consequence is relatively high received echo power so that variations in absorption that might occur near the observation altitudes cannot be distinguished.

Figure 3 shows arrival angle and LOS plasma Doppler velocity at 3290 kHz. The initial phase cannot be identified because it occurs during the ten second VIPIR down time. The main phase of HAAW passage is identified by the downward and upward plasma displacement peaks at $T + 503$ s and $T + 515$ s respectively corresponding to a wave period of 24 s. There is an apparent downward plasma displacement at $T + 534$, but it cannot be positively attributed to the HAAW and the onset time of the tail phase is not determined. The LOS plasma displacements show a structured plasma layer is present before HAAW arrival which could make HAAW induced oscillations difficult to identify. A 4 s

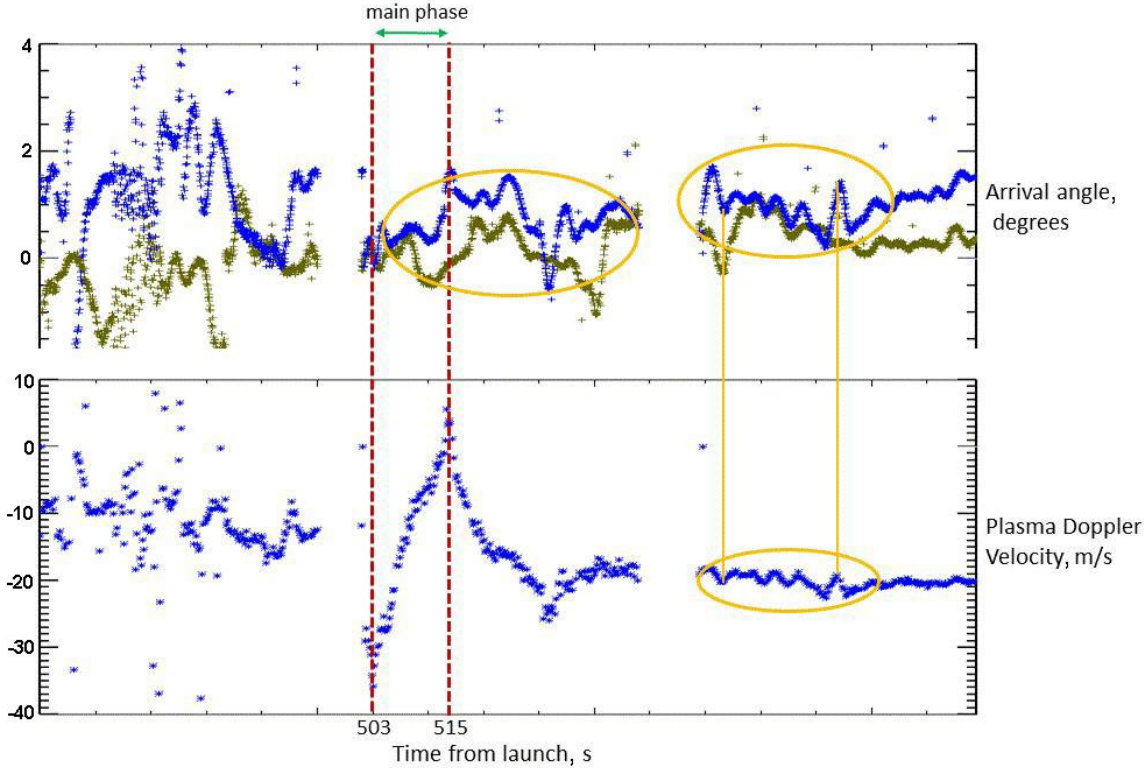

Figure 3. ORB-3 3290 kHz observation of A) arrival angle in the East–West direction (blue) and the North–South direction (green) and B) LOS plasma Doppler velocity. A structured plasma layer is present before HAAW arrival. A 4 s oscillation is present after the main phase.

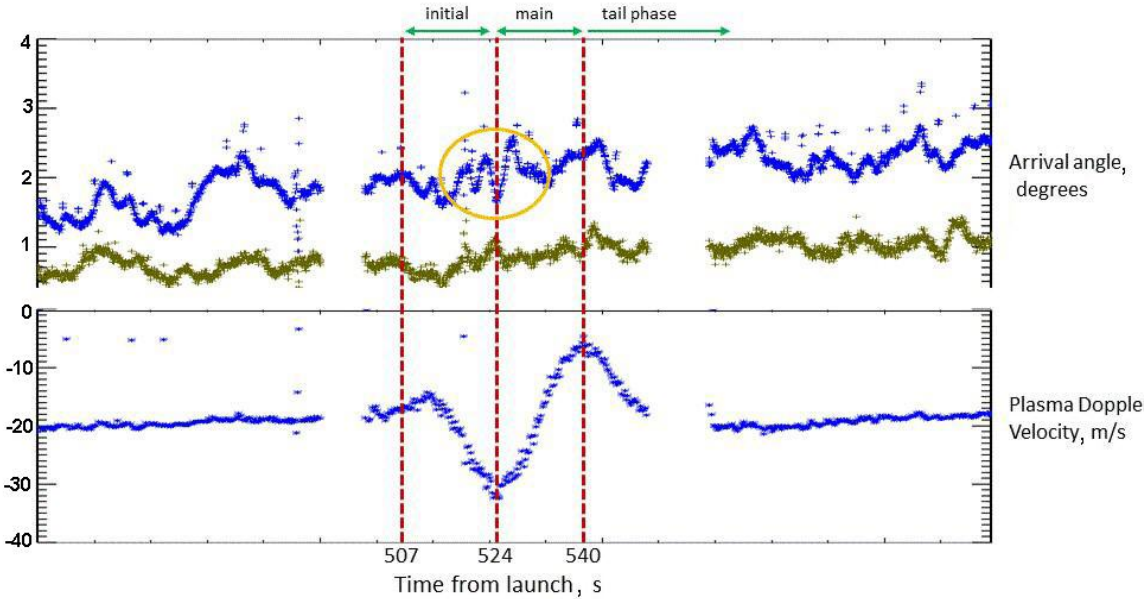

Figure 4. ORB-3 5230 kHz observation of A) arrival angle in the East–West direction (blue) and the North–South direction (green) and B) LOS plasma Doppler velocity. A 4.5 s oscillation is observed during the initial and main phases.

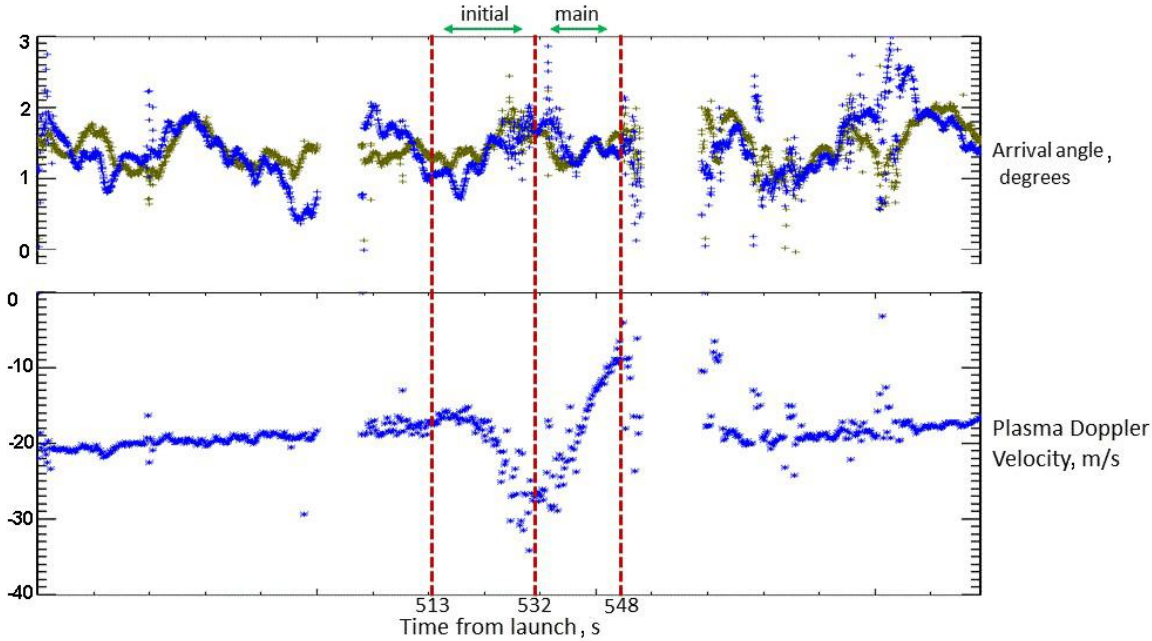

Figure 5. ORB-3 6810 kHz observation of A) arrival angle in the East–West direction (blue) and the North–South direction (green) and B) LOS plasma Doppler velocity. Oscillations are present before HAAW arrival that make possible HAAW induced oscillations difficult to identify. An oscillation near 4.3 s is present in the spectral analysis, but is too obscured by pre-disturbance plasma structure to be visually obvious.

oscillation is present in the $\hat{x}$ direction after the main phase.

Figure 4 shows arrival angle and LOS plasma Doppler velocity at 5230 kHz. The initial phase of HAAW passage begins with the upward plasma displacement beginning at $T + 507$ s. The main phase of HAAW passage is identified by the downward and upward plasma displacement peaks at $T + 524$ s and $T + 540$ s respectively corresponding to a wave period of 32 s. A 4.5 s oscillation is observed during the initial and main phases in the $\hat{x}$ direction.

Figure 5 shows arrival angle and LOS plasma Doppler velocity at 6810 kHz. The initial phase of HAAW passage is identified by the upward plasma displacement beginning at $T+513$ s. The main phase of HAAW passage is identified by the downward and upward plasma displacement peaks at $T+532$ s and $T+548$ s respectively corresponding to a wave period of 32 s. There is an oscillation with a period near 4.3 s in the $\hat{x}$ direction during the initial and main phases. This oscillation can be identified in the spectral analysis, but is too obscured by pre-disturbance plasma structure to be visually obvious.

At all fixed frequency altitudes, HAAW induced plasma displacements having periods consistent PC3

pulsations are observed. Oscillations in arrival angle having periods consistent with PC1 pulsations are also present in the $\hat{x}$ direction at all altitudes but are obscured by other plasma structure in some places.

The ten second period the VIPIR does not transmit during each one-minute observation makes some features difficult to identify including the initial upward plasma displacement peak and the large amplitude downward plasma displacement peak at 3290 kHz, and the large amplitude upward plasma displacement peak at 6820 kHz. The peak LOS plasma displacement speed is comparable at all three altitudes. Because the plasma density increases with altitude, this observation suggests the amount of energy transferred to the geomagnetic field increases with altitude in the bottom side ionosphere with a maximum at the altitude of peak plasma density (h_mF2).

HAAW Induced Oscillations

The rocket induced HAAW originate near the ground, propagate near the adiabatic speed of sound in the lower atmosphere and accelerate away from the adiabatic speed of sound in the F region of the ionosphere.

In the ionosphere, HAAW transfer energy to the surrounding environment [*Artru et al.*, 2004; *Schubert et al.*, 2005], which may cause geomagnetic pulsations.

Oscillations in the wave vector and power observations are determined by spectral analysis. Analysis is performed with a discrete Fourier transform using a Hanning window. The observed periods range from 12 s to 50 s, consistent with the periods of PC3 pulsations.

The plasma displacements that are observed must impact the geomagnetic field according to Maxwell's equations. These plasma displacements have periods that range from 12 s to 50 s, consistent with the periods of PC3 pulsations. These plasma displacements may cause PC3 pulsations like those reported by *Toshihiko et al.* [2005] after an earthquake.

HAAW Induced PC3 Pulsations

The HAAW induced LOS plasma displacements observed in all three experiments have periods that are consistent with PC3 pulsations. The plasma layer rapidly returns to pre-disturbance conditions once the HAAW passes. During ideal MagnetoHydroDynamic (MHD) conditions when the ionosphere can be approximated as stratified, homogeneous and electrically

quasi-neutral, the presented observations would imply a localized disturbance which is a deviation from the electromagnetic steady-state. These plasma displacements are therefore evidence of electric fields that exchange energy with the geomagnetic field.

The observed LOS plasma displacements are determined to be caused by a direct forcing of the neutral atmosphere and they do not themselves provide any information on possible resulting geomagnetic pulsations.

HAAW Induced PC1 Pulsations

In the presented observations, it is determined that variations in HF radio propagation path and absorption occur near the HAAW. These variations have periods that range from about 0.8 s to 5 s, consistent with periods of PC1 geomagnetic pulsations.

In the OA-8 and ORB-1 observations these oscillations are dominant in the signal. When de-trended, the amplitudes of these variations in both arrival angle and received power are nearly constant during times when the periods of oscillation remain constant. These observations can be explained as being caused by PC1 pulsations of the energized geomagnetic field near the HAAW.

The variations in arrival angle and received power in

Figure 1 have a period of 2.5 s during and shortly after the main phase of HAAW passage and a period of 5 s increasing to 7 s during the tail period. This is evidencing the 2.5 s pulsation transitions to the multiple of two 5 s pulsation during the tail period. The latter increase in frequency occurs over time and could be due to decrease in neutral atmosphere density as the HAAW passes. Similarly, in Figure 2 a 0.75 s phase coherent oscillation is observed in arrival angle and received power during the main phase of HAAW passage. After the main phase of HAAW passage a 2.2 s oscillation is observed in received power. This is evidencing a 0.75 s pulsation during the main phase transitions to a multiple of three 2.2 s pulsation after the main phase.

The presented data is interpreted with the understanding that similar oscillations in arrival angle and received power are known to be caused by common HF radio propagation effects [*Wagner,* 1993]. This is particularly challenging with the presented observations because of the limited number of comparable high time resolution fixed frequency soundings of the ionosphere. The evidence that these are caused by geomagnetic pulsations is that to first order: they occur as the HAAW passes through the observed plasma, they are phase coherent in arrival angle and received power, the periods

are constant over multiple oscillations, the periods are consistent with PC1 pulsations, the de-trended peak to peak amplitudes are constant when the period is constant, the oscillations are in the $\hat{x}$ direction and the periods increase by an integer multiple as the HAAW passes.

HAAW Induced PC5 Pulsations

PC5 pulsations observed after earthquakes were identified to occur over timescales comparable to the time it would take for a HAAW to propagate into the ionosphere and be reflected downward and deposit energy in the E region ionosphere [*Toshihiko et al.*, 2005]. Bulk plasma displacements over similar time scales may be caused by large-amplitude HAAW like those that occur after earthquakes [*Zettergren et al.*, 2017]. The expected time scales of both of these mechanisms make them possible causes of HAAW induced PC5 pulsations.

Although the overpressure anomaly of rocket induced HAAW have relatively small amplitudes, the presented results could help understand the effects of large-amplitude HAAW like those that occur after earthquakes. If the observed rocket induced HAAW are downward reflected at higher altitudes, it should be possible to

identify them in the data. Investigation from all experiments yielded no evidence of the observed HAAW being reflected downward. Considering that rocket induced HAAW are smaller in amplitude and propagate in the vertical direction in contrast to seismogenic HAAW, the propagation paths of the two types of HAAW may differ significantly. Specifically, the observed rocket induced HAAW do not appear to be downward reflected whereas seismogenic HAAW have significant horizontal components to their propagation and are expected to be reflected downward [*Zettergren et al.*, 2017]. Additionally, evidence of HAAW induced ionospheric plasma displacements suggests there is plasma transport along the geomagnetic field [*Davies*, 1965]. During large amplitude events, this could cause bulk plasma displacements that could explain previously observed PC5 pulsations. No conclusion is reached on which process is more likely to cause PC5 pulsations, but further experiments using the VIPIR could help resolve this question.

Ground and Space-Based Magnetometers

A significant limitation to the presented observations is the lack of magnetometer observations. Obtaining magnetometer observations of HAAW induced geomag-

netic pulsations after rocket launches should be challenging for several reasons. The presented data show that the disturbances are only detected by the VIPIR for a few tens of seconds near the location of the HAAW neutral atmosphere disturbance. The presented evidence suggests resulting geomagnetic pulsations might be rapidly attenuated and may not be detectable on the ground or at satellite altitudes.

Although the plasma oscillations are only observed near the HAAW, it is possible the geomagnetic pulsations propagate along the field line and may be detectable by ground or space-based magnetometers. Because these relatively low-amplitude HAAW are believed to have a small horizontal spatial extent, the magnetometer would have to be precisely located and be capable of a high observation rate. These requirements eliminate the possibility of space-based observations and observations that leverage permanent ground-based magnetometers.

For ground-based observations, the ideal location would be where the magnetic field line that pierces the point of greatest disturbance amplitude intersects the solid Earth. The greatest disturbance should be directly above the launch site where the ionospheric plasma density is largest (h_mF2). In a future exper-

iment this altitude can be forecast using climatology once a rocket launch is scheduled. This leads to the possibility of deploying a portable magnetometer at the appropriate location.

Plasma Environment in the Ionosphere

The proposed PC1 geomagnetic pulsations can be expressed as ideal MHD waves where the wave frequencies are solutions of the dispersion relation. Future work could compare the presented observations to theoretical computations that make use of parameters derived from atmospheric models like NRLMSISE-00 [*Picone et al.,* 2002]. Any treatment would need to account for model uncertainties, changes in mass density caused by the HAAW itself and limitations of the ideal MHD assumptions [*Boyd and Sanderson,* 2003].

Rather than attempting to find an exact solution, determination of likely wave type is made through analysis of the generalized ideal MHD wave dispersion relations. Specifically, the HAAW induced plasma forcing is determined to be in the vertical direction $\hat{z}$; to first order the geomagnetic field is oriented in the $\hat{y}$ and $\hat{z}$ directions; and plasma oscillations are observed in the $\hat{x}$ direction. This leads to the conclusion that the observed oscilla-

tions are consistent with Shear Alfvén waves.

It was noted that observed frequency shifts appear to occur as integer multiples. This would be consistent with the explanation originally presented by Alfvén which showed they are mathematically equivalent to oscillations of elastic strings. The observed frequency separation between harmonics near 0.5 Hz is consistent with those observed by ground based magnetometers for the low-latitude IAR [*Nosé et al.*, 2017]. The ORB-1 frequency separation of 0.7 Hz is higher than those observations, but the WFF VIPIR is a mid-latitude instrument and the prior observations are not expected to include all possible frequency shifts.

Summary and Future Plans

The following is what appears to be most consistent with the presented observations: The HAAW neutral pressure anomaly causes plasma displacements which drive PC3 type geomagnetic pulsations; and energy transferred to the geomagnetic field by the HAAW causes the geomagnetic field to generate PC1 pulsations. These PC1 pulsations originate with higher frequency harmonics transitioning to lower frequency harmonics as the geomagnetic field sheds the HAAW induced energy.

The presented VIPIR ionosonde observations show characteristics of PC1 and PC3 geomagnetic pulsations and may help explain previously observed PC5 pulsations. These observations are presented in the context of earlier observations of seismogenic HAAW induced geomagnetic pulsations. One next step would be to model the observed HAAW induced plasma displacements and to make more observations during missions of opportunity like future rocket launches. A future experiment could reproduce the presented experimental method with the addition of a temporary magnetic observatory at the location where the geomagnetic field line which pierces the observed plasma intersects with the solid Earth. An important tool for making high quality future observations would be an automated method to make similar VIPIR observations when large earthquakes occur.

Acknowledgments. This work is supported by the National Aeronautics and Space Administration grant No. NNX09AI76G. The author thanks Terence Bullett for his support and help in making the presented observations, and Tatiana Sazonova for her support and help in drafting this manuscript. Data used in support of this work can be obtained from the NOAA National Centers for Environmental Information ionosonde@noaa.gov.

References

Artru, J., T. Farges, P. Lognonne (2004), Acoustic waves generated from seismic surface waves: propagation properties determined from Doppler sounding observations and normal-mode modelling, *Geophys. J. Int.*, *158*, p. 1067–1077, **Crossref**

Bianchi, C., D. Altadill (2005), Ionospheric Doppler measurements by means of HF-radar techniques, *Annals of Geophysics*, *48*, p. 6.

Boyd, T. J. M., J. J. Sanderson (2003), *The Physics of Space Plasmas*, Cambridge Univ. Press, Cambridge (ISBN 0 521 45912 5).

Davies, K. (1965), *Ionospheric Radio Propagation*, United States Department of Commerce National Bureau of Standards, Library of Congress Catalog Card Number: 64-60061, US.

Mabie, J., T. Bullett, P. Moore, G. Vieira (2016), Identification of rocket-induced acoustic waves in the ionosphere, *Geophys. Res. Lett.*, *43*, **Crossref**

Maruyama, T., T. Tsugawa, H. Kato, M. Ishii, M. Nishioka (2012), Rayleigh wave signature in ionograms induced by strong earthquakes, *J. Geophys. Res.*, *117*, p. A08306, **Crossref**

Negrea, C. N., N. Zabotin (2016), Mean spectral characteristics of acoustic gravity waves in the thermosphere-ionosphere determined from Dynasonde data, *Radio Science*, *51*, p. 213–222, **Crossref**

Negrea, C., N. Zabotin, T. Bullett, T. Fuller-Rowell, T. Fang, M. Codrescu (2016), Characteristics of acoustic gravity waves obtained from Dynasonde data, *J. of Geophys. Res. Space*

Physics, *121*, p. 3665–3680, **Crossref**

Nosé, M., M. Uyeshima, J. Kawai, H. Hase (2017), Ionospheric Alfvén resonator observed at low-latitude ground station Muroto, *J. Geophys. Res. Space Physics*, *122*, **Crossref**

Pederic, L. H., M. A. Cervera (2014), Semiempirical model for ionospheric absorption based on the NRLMSISE-00 atmospheric model, *Rad. Sci.*, *49*, p. 81–93, **Crossref**

Picone, J. M., A. E. Hedin, D. P. Drob, A. C. Aikin (2002), NRLMSISE-00 empirical model of the atmosphere: Statistical comparison and scientific issues, *Journal of Geophysical Research: Space Physics*, *107*, no. A12, p. 1468, **Crossref**

Pitteway, M., J. Wright (1992), Toward and optimum receiving array and pulse set for the Dynasonde, *Rad. Sci.*, *27*, no. 4, p. 481–490, **Crossref**

Saito, T. (1978), Long-period irregular magnetic pulsation, Pi3, *Space Science Reviews*, *21*, p. 427–467, **Crossref**

Schubert, G., M. P. Hickey, R. L. Waltersheid (2005), Physical processes in acoustic wave heating of the thermosphere, *J. Geophys. Res.*, *110*, p. D07106, **Crossref**

Scotto, C., A. Settimi (2014), The calculation of ionospheric absorption with modern computers, *Adv. Space Res.*, *54*, p. 1642–1650, **Crossref**

Sutcliffe, P. R., M. J. Jarvis (1996), The phase relationships of the ionospheric signatures of Pc1 geomagnetic pulsations, *J. Atmos. Terr. Phys.*, *58*, no. 15, p. 1783–1792, **Crossref**

Toshihiko, I., et al. (2005), Geomagnetic pulsations caused by the Sumatra earthquake on December 26, 2004, *Geophys. Res.*

Lett., *32*, p. L20807, **Crossref**

Yagova, N., B. Heilig, E. Fedorov (2015), Pc2–3 geomagnetic pulsations on the ground, in the ionosphere, and in the magnetosphere: MM100, CHAMP, and THEMIS observations, *Annales Geophysicae*, *33*, p. 117–128, **Crossref**

Wagner, L. S. (1993), *Morphology and characteristics of disturbed HF skywave channels, Naval Research Laboratory Bulletin, NRL Transmission Technology Branch Information Technology Division, Bulletin NRL/MR/5554-93-7389*, Naval Research Laboratory, US.

Wickersham, A. F. Jr. (1966), Identification of acoustic-gravity wave modes from ionospheric range-time obsersvations, *J. Geophys. Res.*, *71*, no. 19, p. 4551–4555, **Crossref**

Zabotin, N. A., J. W. Wright, G. A. Zhbankov (2006), NeXtYZ: Three-dimensional electron density inversion for dynasonde ionograms, *Radio Science*, *41*, p. 6, **Crossref**

Zettergren, M. D., J. B. Snively, A. Komjathy, O. P. Verkhoglyadova (2017), Nonlinear ionospheric responses to large-amplitude infrasonic-acoustic waves generated by undersea earthquakes, *J. Geophys. Res. Space Physics*, *122*, **Crossref**